Temperature and pressure dependence of the luminescence of Eu^{2+}-doped fluoride crystals $Ba_xSr_{1-x}F_2$ (x = 0, 0.3, 0.5 and 1): experiment and model

2009 J. Phys.: Condens. Matter 21 245601

(http://iopscience.iop.org/0953-8984/21/24/245601)

J. Phys.: Condens. Matter **21** (2009) 245601 (12pp) doi:10.1088/0953-8984/21/24/245601

Temperature and pressure dependence of the luminescence of Eu^{2+}-doped fluoride crystals $Ba_xSr_{1-x}F_2$ ($x = 0$, 0.3, 0.5 and 1): experiment and model

S Mahlik[1], K Wiśniewski[1], M Grinberg[1] and R S Meltzer[2]

[1] Institute of Experimental Physics, University of Gdańsk, Wita Stwosza 57, 80-952 Gdańsk, Poland
[2] Department of Physics and Astronomy, University of Georgia, Athens, GA 30602, USA

Received 10 January 2009, in final form 29 April 2009
Published 21 May 2009
Online at stacks.iop.org/JPhysCM/21/245601

Abstract

This paper summarizes experimental evidence of anomalous luminescence in Eu^{2+}-doped fluoride crystals $Ba_xSr_{1-x}F_2$ ($x = 0$, 0.3, 0.5 and 1). Luminescence, luminescence excitation spectra and luminescence kinetics obtained at ambient and high hydrostatic pressure at various temperatures are discussed. Hydrostatic pressure was shown to cause a redshift of normal $4f^65d^1(e) \rightarrow 4f^7$ emission and anomalous luminescence. The experimental data shows the existence of temperature- and pressure-induced spectral transformations where the anomalous luminescence is replaced by normal emission of Eu^{2+} centers. We present a model that predicts a strong electron–lattice coupling of the trapped excitons as well as the pressure effect of the spectral transformation from anomalous to normal emission.

1. Introduction

Luminescence of fluoride crystals (XF_2, where X = Ca, Sr and Ba) doped with Eu^{2+} is dominated either by broad band blue luminescence, related to the internal $4f^65d^1(e) \rightarrow 4f^7$ transition in the Eu^{2+} ion (SrF_2:Eu^{2+} (Moine *et al* 1994) and CaF_2:Eu^{2+} (Troster *et al* 2002)) or anomalous yellow luminescence related to recombination of the Eu^{2+} trapped exciton in BaF_2:Eu^{2+} (Moine *et al* 1994). The different luminescence lineshapes in different crystals have been related to the relative energy of the $4f^65d^1(e)$ state with respect to the conduction band (Moine *et al* 1991). It has been argued that the energy of the $4f^65d^1(e)$ state is below the conduction band edge in SrF_2:Eu^{2+} and is degenerate with the conduction band in the case of BaF_2:Eu^{2+} (Moine *et al* 1991).

An interesting effect has been observed in mixed crystals of $Ba_xSr_{1-x}F_2$:Eu^{2+} where the luminescence lineshape has been found to be dependent on material composition (Dujardin *et al* 1992, Gatch *et al* 2006). Specifically, for an amount of Ba larger than 30 at.% ($x > 0.3$) the emission spectrum was dominated by anomalous emission whose peak energy was shifted to the blue with respect to pure BaF_2:Eu^{2+} and the shift increased with an increase of Sr concentration.

The appearance of anomalous luminescence instead of the $4f^{n-1}5d^1 \rightarrow 4f^n$ luminescence has been observed in several materials doped with divalent Eu^{2+} and Yb^{2+}. Examples include BaF_2:Eu^{2+}, CaF_2:Yb^{2+} (Reut 1978), (CaSr)$MgSi_2O_7$:Eu^{2+} (Poot and Blasse 1997), BaS:Eu^{2+} (Smet *et al* 2006) and Sr_2SiO_4:Eu^{2+} (Kim *et al* 2005). The problem of anomalous luminescence in materials doped with Eu^{2+} and Yb^{2+} has been reviewed in Dorenbos (2003). Photocurrent experiments (Pedrini *et al* 1979, 1981) have shown a relationship between the existence of anomalous luminescence and the ionization of rare earth ions (McClure and Pedrini 1985), which led to the development of a model of the impurity trapped excitons, wherein a hole is captured at the lanthanide ion and an electron is delocalized at the neighboring metal ions (Dorenbos 2003).

Since anomalous luminescence is a common effect we performed a more detailed study of the problem. The main goal was to formulate a quantitative model of the impurity trapped exciton which could explain the major experimental details. In our previous paper, (Mahlik *et al* 2008) we have shown that the absorption and excitation spectra of BaF_2:Eu^{2+}, $Ba_xSr_{1-x}F_2$:Eu^{2+} and SrF_2:Eu^{2+} consist of well-defined $4f^7 \rightarrow 4f^65d^1(e)$ and $4f^7 \rightarrow 4f^65d^1(t_2)$ transitions

over the whole composition range. Since one has shown separate identifiable bands, both excited states, $4f^6 5d^1(e)$ and $4f^6 5d^1(t_2)$, must lie in the bandgap of the material and are not degenerate with the conduction band.

We have measured the effect of pressure on the trapped exciton states and luminescence lineshapes in $SrF_2:Eu^{2+}$, $BaF_2:Eu^{2+}$ and $Ba_xSr_{1-x}F_2:Eu^{2+}$ (Gatch *et al* 2006). In the case of $SrF_2:Eu^{2+}$ we have obtained a negative pressure shift for the $4f^6 5d^1(e) \rightarrow 4f^7$ luminescence ($-17.4\ cm^{-1}\ kbar^{-1}$ in the range 1–60 kbar and approximately zero for higher pressure). In the case of $BaF_2:Eu^{2+}$ and the mixed crystal $Ba_{0.3}Sr_{0.7}F_2:Eu^{2+}$, where at ambient conditions the anomalous luminescence was present, we have noticed quite large negative pressure shifts of the anomalous emission ($-16.3\ cm^{-1}\ kbar^{-1}$ for $BaF_2:Eu^{2+}$ and approximately $-20\ cm^{-1}\ kbar^{-1}$ for $Ba_{0.3}Sr_{0.7}F_2:Eu^{2+}$). At pressures of 39 kbar and 40 kbar for $BaF_2:Eu^{2+}$ and $Ba_{0.3}Sr_{0.7}F_2:Eu^{2+}$, respectively, the anomalous luminescence was replaced by normal $4f^6 5d^1(e) \rightarrow 4f^7$ emission whose energy decreased with pressure at a rate of $-14\ cm^{-1}\ kbar^{-1}$ and $-8.2\ cm^{-1}\ kbar^{-1}$, respectively. Replacement of anomalous luminescence by normal luminescence has been attributed to a pressure-induced cubic to orthorhombic phase transition that takes place at 30 kbar (Leger *et al* 1995) and 50 kbar (Kourouklis and Anatassakis 1986, Francisco *et al* 2002), for BaF_2 and SrF_2, respectively.

The influence of the pressure-induced cubic to orthorhombic phase transition on Mn^{2+} luminescence has been studied in $CaF_2:Mn^{2+}$, $Ca_{0.5}Sr_{0.5}F_2:Mn^{2+}$ (Rodriguez *et al* 2003), $SrF_2:Mn^{2+}$ and $BaF_2:Mn^{2+}$ (Hernández and Rodriguez 2003). The decrease of the emission energy and luminescence lifetime were assigned to an increase in the crystal field.

However, detailed analysis of the pressure and temperature dependence of the luminescence lineshape in $BaF_2:Eu^{2+}$ has shown that, in fact, there exists a smooth pressure-induced level crossing of the $4f^6 5d^1(e)$ state and impurity trapped exciton states, that takes place in the cubic phase at pressures below the phase transition (Mahlik *et al* 2008).

Since the ionic radius of Ba^{2+}, equal to 1.42 Å for dodecahedral coordination, is larger than the ionic radius of Sr^{2+} (1.26 Å) (Shannon 1976), one expects that a decrease in the Ba content should be equivalent to an increase of pressure. This general rule of equivalence of hydrostatic pressure and chemical pressure is contradictory to the experimental results where an increase of pressure diminished the energy of anomalous luminescence and an increase of Ba content causes the same effect.

In this paper we present experiments on the pressure and temperature dependence of the luminescence and luminescence kinetics of Eu^{2+}-doped $Ba_xSr_{1-x}F_2$ ($x = 0$, 0.3, 0.5 and 1) mixed crystals. The new results are compared with those obtained previously in $BaF_2:Eu^{2+}$ and $SrF_2:Eu^{2+}$. We discuss the earlier model of the impurity trapped exciton and use it to formulate the qualitative conditions for the existence of the impurity trapped exciton. Also the influence of the cubic to orthorhombic phase transition on the formation of the impurity trapped exciton states and the luminescence lineshapes is discussed.

2. Experimental technique

2.1. Steady state luminescence

The luminescence was excited with a CW HeCd laser at a wavelength of 325 nm, corresponding to the excitation of the $4f^6 5d^1(e)$ state of Eu^{2+}. The luminescence was detected with a multichannel analyzer OMA system (S-1000 spectrometer made by Ocean Optics). To obtain low temperature emission spectra the samples were cooled in a closed-cycle helium refrigerator. All emission spectra were corrected for the instrumental response.

2.2. Time-resolved luminescence

The luminescence kinetics was measured at room temperature using a Hamamatsu C4334-01 model Streak Camera. The luminescence was spectrally separated with a Bruker Optics 2501S model monochromator. To obtain the time dependence of the emission, samples were excited with an optical parametric generator PG401/SH pumped by the tripled output of a pulsed Nd:YAG laser.

2.3. High pressure technique

High pressure experiments were performed in a diamond anvil cell (DAC) (Dunstan and Spain 1989). The sample was placed in a hole drilled in a metal gasket between two parallel diamond anvils. Pressure appears when the diamonds are moved and is transmitted to the fluid medium. A ruby crystal was used as the pressure detector. Two systems were used for force generation; the Merrill–Bassett system (Merrill and Bassett 1974) and one designed by Diacell Products Ltd. In both of these, the plates with diamonds are joined with screws controlling the distance between the anvils.

3. Experimental results

3.1. Temperature dependence of luminescence of $Ba_xSr_{1-x}F_2:Eu^{2+}$ ($x = 0$, 0.3, 0.5 and 1) at ambient pressures

Ambient pressure luminescence spectra obtained at different temperatures for macroscopic samples of $Ba_xSr_{1-x}F_2:Eu^{2+}$ for $x = 0$, 0.3, 0.5 and 1 are presented in figures 1(a)–(d), respectively. The intensity of the luminescence was measured at different temperatures under the same excitation conditions so that the relative integrated intensities can be used to analyze the dependence of the luminescence efficiency on temperature.

In the case of $SrF_2:Eu^{2+}$ the luminescence results from the $4f^6 5d^1(e) \rightarrow 4f^7$ transition peaked at 24 100 cm^{-1} with a half-width approximately equal to 1400 cm^{-1}. The integrated intensity was constant for temperatures below 270 K and decreased slightly at room temperature.

In the $Ba_xSr_{1-x}F_2$ ($x = 0.3$ and 0.5) crystals doped with Eu^{2+}, the anomalous luminescence competed with the normal $4f^6 5d^1(e) \rightarrow 4f^7$ emission and the actual luminescence lineshape depended on temperature. In the case of $Ba_{0.3}Sr_{0.7}F_2:Eu^{2+}$ the emission intensity was almost constant for temperatures below 200 K and then decreased

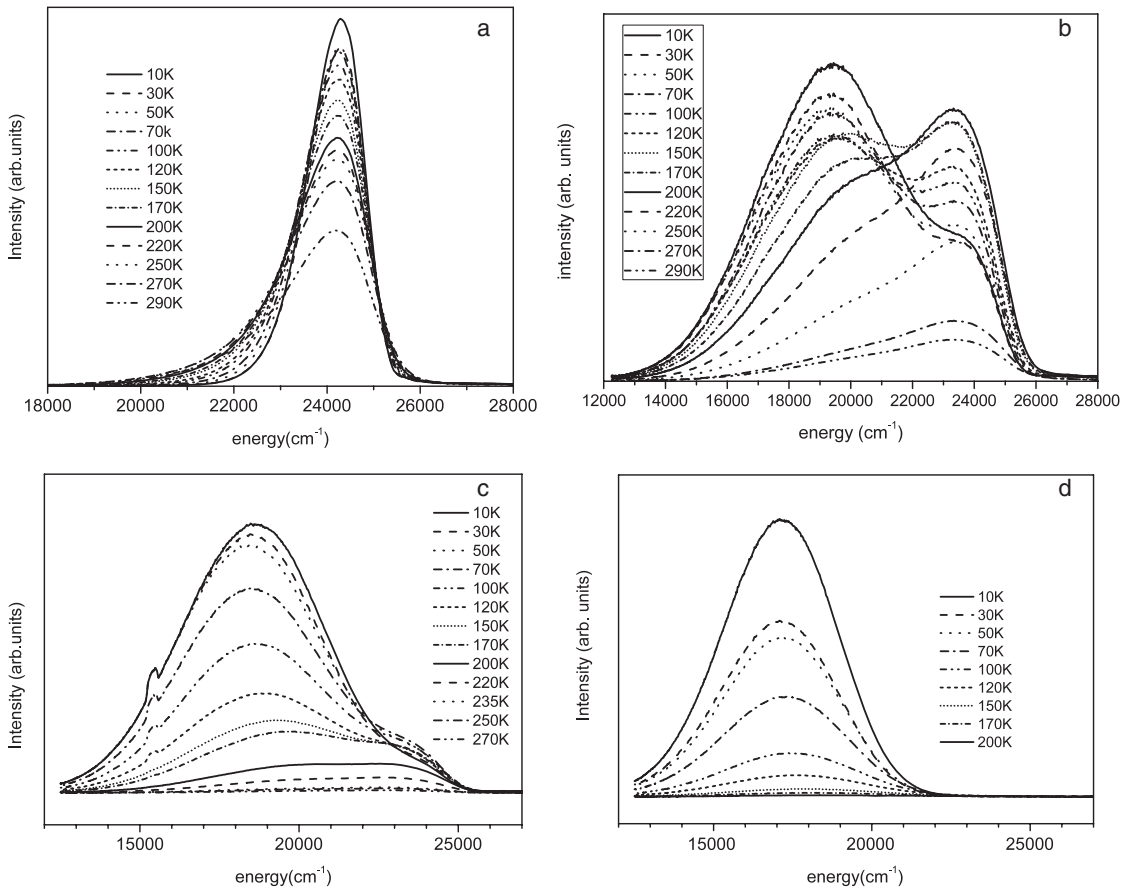

Figure 1. Ambient pressure luminescence spectra obtained at different temperature for $Ba_xSr_{1-x}F_2$:Eu^{2+} for $x = 0$ (a), $x = 0.3$ (b), $x = 0.5$ (c) and $x = 1$ (d).

rapidly for higher temperatures. At low temperatures the emission consisted of a broad band peaked at 19 100 cm^{-1} related to emission of the Eu^{2+} trapped exciton, whereas for higher temperatures the luminescence was dominated by the sharper $4f^6 5d^1(e) \rightarrow 4f^7$ emission peaked at 23 300 cm^{-1}. In the case of $Ba_{0.5}Sr_{0.5}F_2$:Eu^{2+} the luminescence intensity decreased above 50 K; the exciton emission was peaked at 18 260 cm^{-1} and the $4f^6 5d^1(e) \rightarrow 4f^7$ luminescence was peaked at 23 000 cm^{-1}.

In the case of BaF_2:Eu^{2+} the emission intensity consisted of a single broad band peaked at 16 700 cm^{-1} related to the Eu^{2+} trapped exciton whose intensity decreased strongly with increasing temperature. In figure 1(d) the luminescence for temperatures higher than 200 K is not presented due to the fact that our detection system (OMA) was not sensitive enough for detection of the weak luminescence at higher temperature. It is known, however, that for temperatures above 200 K the emission related to the $4f^6 5d^1(e) \rightarrow 4f^7$ luminescence of Eu^{2+}, peaked at 23 500 cm^{-1}, is also seen (Mahlik *et al* 2008).

The integrated intensities of the spectra versus temperature are presented in figure 2(a). The intensity of the emission spectra of BaF_2:Eu^{2+} and mixed crystals decrease with temperature. This effect is related to the nonradiative internal conversion process (intersystem crossing process) that involves mainly the Eu^{2+} trapped exciton state and the ground state of the Eu^{2+}. We can reproduce the dependence of the integrated emission intensity on temperature using the following formula:

$$I = \frac{1}{1 + P_1\tau_R \exp[\frac{-\delta_1}{kT}] + P_2\tau_R \exp[\frac{-\delta_2}{kT}]} \qquad (1)$$

which presents the ratio of intensity at temperature T to the intensity at 0 K. According to (1) two deexcitation pathways related to intersystem crossing are considered. The configurational coordinate diagram corresponding to formula (1) is presented in figure 2(b). The pathway labeled '1' corresponds to the classical effect of thermal activation over an energy barrier, δ_1. The pathway labeled '2', characterized by activation energy δ_2 and probability P_2, corresponds to the tunneling of the system from the excited to the ground electronic manifold after excitation to the first excited vibronic state of the excited electronic manifold.

The effect of the tunneling in the first excited vibronic state is important only in the case when the barrier is not too thick and not too high to allow tunneling. This occurs when there is a large electron–lattice coupling and when the excited state parabola is strongly shifted in configurational space with respect to the ground state. The barrier height and thickness can be calculated when parameters of the ground and excited parabolas are known. They depend on the electron–lattice coupling energy and energy of the excited state, related to the horizontal and vertical shifts of the excited parabola,

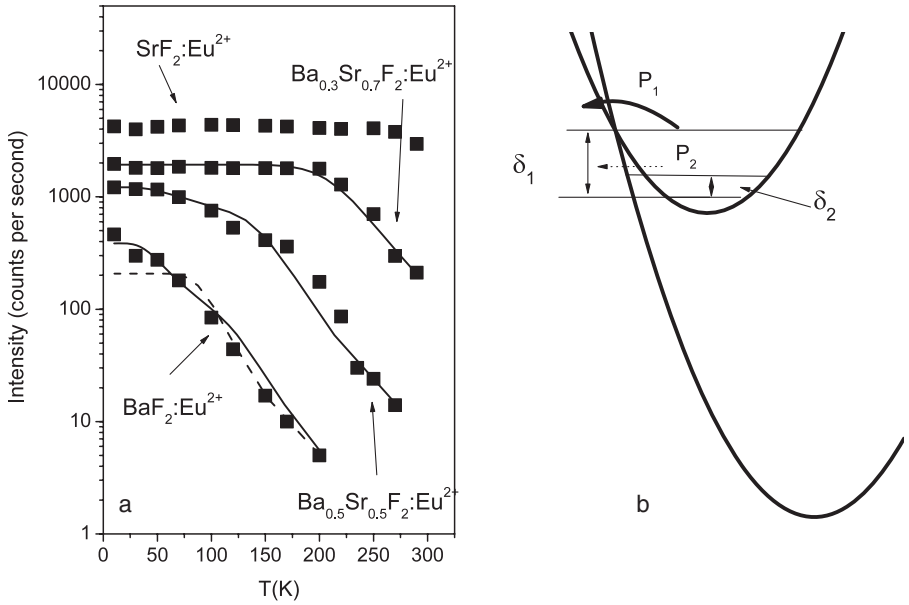

Figure 2. (a) The integrated intensities of the spectra versus temperature for $Ba_xSr_{1-x}F_2:Eu^{2+}$ for $x = 0$, 0.3, 0.5 and 1. Solid curves represent the fitting obtained according to formula (1), the dashed curve corresponds to the fitting according to formula (1) under the assumption $P_2 = 0$. (b) A configurational coordinate diagram representing nonradiative interconfigurational transition (intersystem crossing) in the system with strong lattice relaxation.

Table 1. Parameters describing the nonradiative processes in the Eu^{2+} trapped exciton system. Fits have been performed considering the radiative lifetime $\tau_R = 1.27$ μs (see discussion in section 3.3).

	δ_2 (cm^{-1})	P_2 (10^6 s^{-1})	δ_1 (cm^{-1})	P_1 (10^9 s^{-1})
$BaF_2:Eu^{2+}$	—	0	1100	3.37
$BaF_2:Eu^{2+}$	270	16.0	1700	17.4
$Ba_{0.5}Sr_{0.5}F_2:Eu^{2+}$	270	2.3	2200	17.4
$Ba_{0.3}Sr_{0.7}F_2:Eu^{2+}$	270	0	3400	17.4

respectively. In the case of $BaF_2:Eu^{2+}$ the energy of the excited parabola is smaller than in the case of $Ba_{0.3}Sr_{0.7}F_2:Eu^{2+}$. As a result, in $BaF_2:Eu^{2+}$ the activation energy δ_1 is smaller and the barrier is thinner than in $Ba_{0.3}Sr_{0.7}F_2:Eu^{2+}$. Thus, in $BaF_2:Eu^{2+}$, tunneling from the first excited vibronic state is important whereas in $Ba_{0.3}Sr_{0.7}F_2:Eu^{2+}$ the influence of tunneling is negligible. We fitted the data to formula (1) as follows. We started the fitting with $Ba_{0.3}Sr_{0.7}F_2:Eu^{2+}$ where we obtained a very good fit for $P_2 = 0$. From this fit we obtained δ_1 and P_1. Then the resulting value of P_1 was kept constant for the other systems. The value of δ_2 was obtained by fitting the $BaF_2:Eu^{2+}$ luminescence damping and was kept constant for other fits. The parameters resulting from the fitting are presented in table 1. We were not able to fit the experimental data for $BaF_2:Eu^{2+}$ using one activation energy. The best fitting for $BaF_2:Eu^{2+}$, obtained with fixed $P_2 = 0$, is represented by the dashed curve in figure 2(a).

The energy barrier δ_1 increases with a decrease in the amount of Ba and is accompanied by an increase of the energy of the trapped exciton state. This is in full accordance with the configurational model where the activation energy of intersystem crossing increases with increasing energy of the excited electronic manifold.

3.2. Temperature dependence of luminescence in $Ba_xSr_{1-x}F_2:Eu^{2+}$ ($x = 0.3$, 0.5) for different pressures

The emission spectrum of $SrF_2:Eu^{2+}$ consists of the band related to normal $4f^65d^1(e) \rightarrow 4f^7$ emission for all investigated pressures and temperatures (Gatch *et al* 2006). The emission spectra of $BaF_2:Eu^{2+}$ obtained at different pressures and temperatures have been presented in Mahlik *et al* (2008). The results show that, when the pressure increases, the normal $4f^65d^1(e) \rightarrow 4f^7$ emission begins to appear at lower temperatures, and for pressures greater than 33 kbar only the normal $4f^65d^1(e) \rightarrow 4f^7$ emission is observed at all temperatures. This effect was attributed to the crossover in energy of the trapped exciton and $4f^65d^1(e)$ states. It was demonstrated that high pressure transforms the anomalous luminescence into normal emission in $Ba_{0.3}Sr_{0.7}F_2:Eu^{2+}$ (Gatch *et al* 2006). However, in this case, the above explanation was not obvious as the relative intensities of both kinds of luminescence, anomalous and normal, were weakly independent of pressure in the broad range of pressures.

In order to analyze the difference between the energy of the $4f^65d^1(e)$ state and that of the trapped exciton state, luminescence was measured at various pressures and temperatures for $Ba_xSr_{1-x}F_2:Eu^{2+}$ ($x = 0.3$ and 0.5). The selected spectra are presented in figures 3(a), (b) and 4(a) and (b) for $Ba_{0.3}Sr_{0.7}F_2:Eu^{2+}$ and $Ba_{0.5}Sr_{0.5}F_2:Eu^{2+}$, respectively. We consider that the spectra are superpositions of two bands related to normal and anomalous luminescence. In figure 5 the energies of the respective luminescence peaks (the energies of local maxima taken from the spectra) versus pressure for all considered materials are presented. The energies and pressure shifts are listed in table 2. The averaged quantities of the shifts are similar, as reported earlier (Gatch *et al*

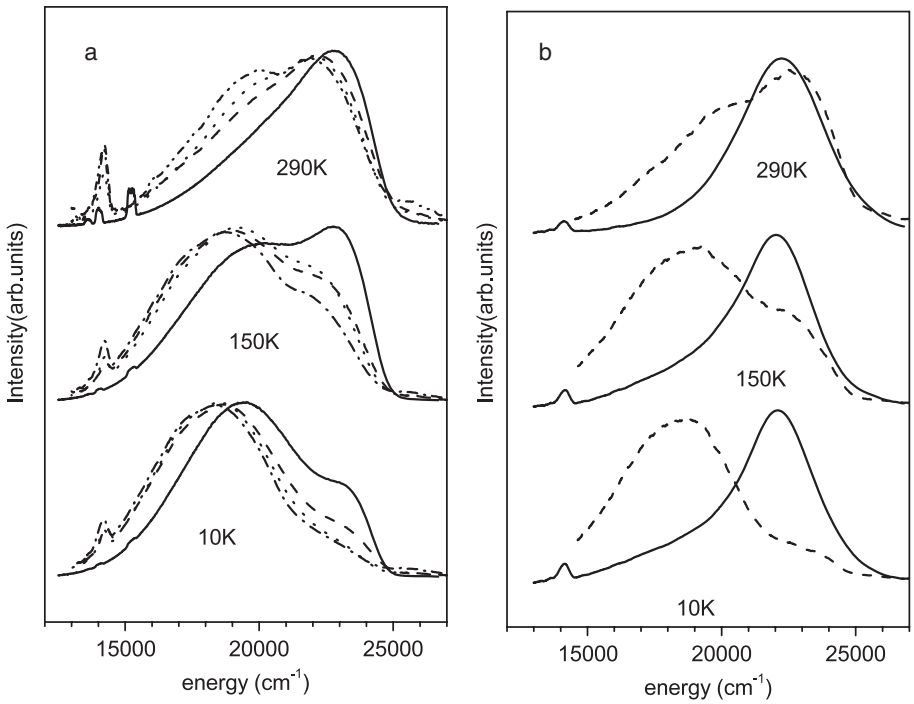

Figure 3. Luminescence spectra of $Ba_{0.3}Sr_{0.7}F_2:Eu^{2+}$ for different temperatures and pressures. All spectra are normalized to the maximum. (a) The spectra for ambient pressure (solid curves), 7 kbar (dashed curves), 20 kbar (dotted curves) and 27 kbar (dashed–dotted curves). (b) The spectra for 35 kbar (dashed curves) and 40 kbar (solid curves).

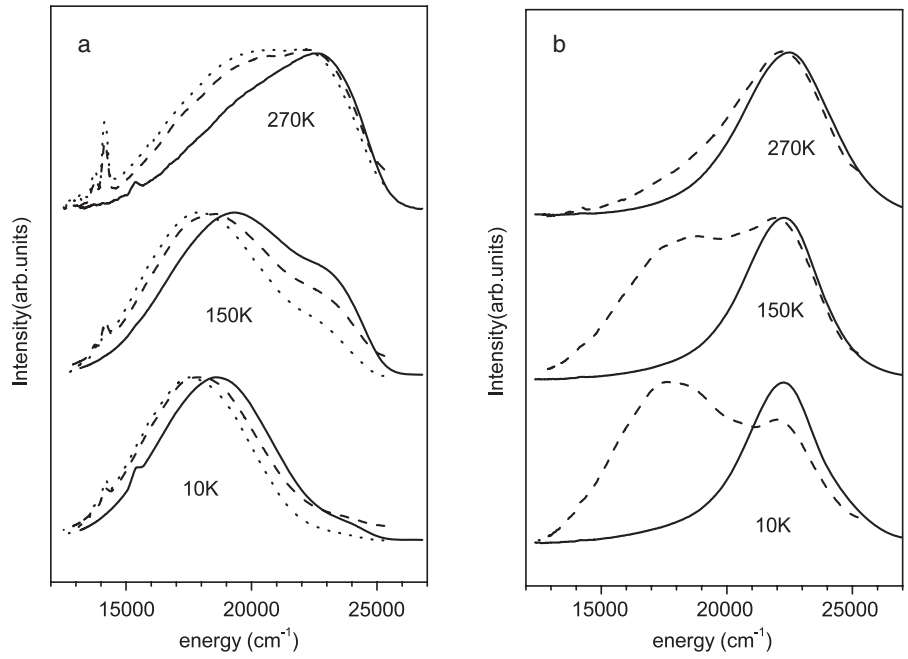

Figure 4. Luminescence spectra for $Ba_{0.5}Sr_{0.5}F_2:Eu^{2+}$ for different temperatures and pressures. All spectra are normalized to the maximum value. (a) The spectra for ambient pressure (solid curves), 11 kbar (dashed curves), 21 kbar (dotted curves). (b) The spectra for 29 kbar (dashed curves) and 36 kbar (solid curves).

2006). The new results show additionally that in the case of the anomalous luminescence the pressure shifts decrease with increasing pressure.

Considering the spectra in figures 3 and 4 one notices that for both materials at ambient pressure at low temperature the luminescence is dominated by broad band emission related to the Eu^{2+} trapped exciton, and with increasing temperature the relative contribution from $4f^6 5d^1(e) \rightarrow 4f^7$ emission increases. A similar effect has been observed in the case of $BaF_2:Eu^{2+}$ (Gatch *et al* 2006, Mahlik *et al* 2008), but in the case of mixed crystals $Ba_xSr_{1-x}F_2:Eu^{2+}$ it is stronger.

Table 2. Energies and pressure shifts of the luminescence bands. For BaF_2:Eu^{2+} all data are taken from the spectra obtained at 10 K. For other crystals data for anomalous luminescence was obtained at 10 K, while data for normal d–f luminescence was obtained at room temperature (290 K).

	Exciton luminescence		$4f^6 5d^1(e) \rightarrow 4f^7$	
	E at $p = 1$ bar (cm^{-1})	$\frac{dE}{dp}$ (cm^{-1} $kbar^{-1}$)	E (cm^{-1})	$\frac{dE}{dp}$ (cm^{-1} $kbar^{-1}$)
BaF_2:Eu^{2+}	16 700	−14.0	22 300	−16.3
$Ba_{0.5}Sr_{0.5}F_2$:Eu^{2+}	18 260	−45.0 ($p < 20$ kbar) 4.0 ($p > 20$ kbar)	23 000 ($p = 1$ bar) 22 450 ($p = 30$ kbar)	−13.0 ($p < 20$ kbar) 4.0 ($p > 30$ kbar)
$Ba_{0.3}Sr_{0.7}F_2$:Eu^{2+}	19 100	−55 ($p < 15$ kbar) −14.0 ($p > 15$ kbar)	23 300	−7.2
SrF_2:Eu^{2+}	—	—	24 100 ($p = 1$ bar) 23 150 ($p = 40$ kbar)	−17.3 ($p < 60$ kbar) 0 ($p > 60$ kbar)

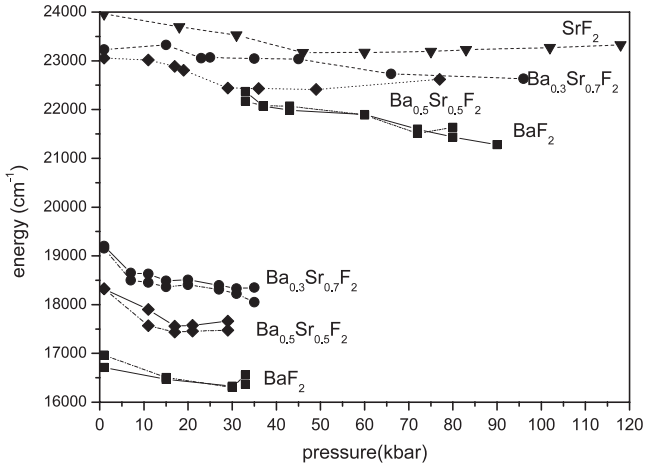

Figure 5. Energies of the trapped exciton and $4f^6 5d^1(e) \rightarrow 4f^7$ luminescence for different pressures and temperatures. Symbols (rectangle ■), (rhomb ♦), (circle ●) and (triangle ▼) represent data obtained for BaF_2:Eu^{2+}, $Ba_{0.5}Sr_{0.5}F_2$:Eu^{2+}, $Ba_{0.3}Sr_{0.7}F_2$:Eu^{2+} and SrF_2:Eu^{2+}, respectively. Solid, dashed–dotted, dotted and dashed lines represent data obtained at 10 K, 50 K, 250 K and room temperature, respectively. The data for BaF_2:Eu^{2+} and SrF_2:Eu^{2+} has been taken from Gatch *et al* (2006).

As in BaF_2:Eu^{2+} (Gatch *et al* 2006, Mahlik *et al* 2008), one concludes that at ambient pressure the energy of the $4f^6 5d^1(e)$ state is greater than that of the Eu^{2+} trapped exciton state. This situation is similar to that observed for pressures lower than 40 kbar and 36 kbar for $Ba_{0.3}Sr_{0.7}F_2$:Eu^{2+} and $Ba_{0.5}Sr_{0.5}F_2$:Eu^{2+}, respectively. For higher pressures, only the $4f^6 5d^1(e) \rightarrow 4f^7$ emission is observed in both materials. The total luminescence intensity (I_{tot}) is a superposition of exciton emission (labeled I_{ex}) and $4f^6 5d^1(e) \rightarrow 4f^7$ luminescence (labeled I_{d-f}). Assuming occupation of the Eu^{2+} trapped exciton state and $4f^6 5d^1(e)$ state are in thermal equilibrium, one obtains

$$I_{tot} = I_{ex} + I_{d-f} \propto \frac{1}{\tau_{ex}} + \frac{1}{\tau_{d-f}} \exp\left(-\frac{\delta}{kT}\right) \qquad (2)$$

where energy δ is the difference between energies of the $4f^6 5d^1(e)$ state and the Eu^{2+} trapped exciton state, and τ_{ex} and τ_{d-f} are radiative decay times of the exciton and $4f^6 5d^1(e) \rightarrow 4f^7$ emission, respectively. Relation (2) allows one to calculate the ratio of the $4f^6 5d^1(e) \rightarrow 4f^7$ intensity to the intensity of the Eu^{2+} trapped exciton emission:

$$\frac{I_{d-f}}{I_{ex}} = \frac{\tau_{ex}}{\tau_{d-f}} \exp\left(-\frac{\delta}{kT}\right). \qquad (3)$$

Considering the spectra presented in figures 1(a)–(c) in relation to equation (3) one notices that at ambient pressure the energy δ increases with increasing Ba content. Very interesting results are obtained for the pressure range below 36 kbar and 29 kbar for $Ba_{0.3}Sr_{0.7}F_2$:Eu^{2+} and $Ba_{0.5}Sr_{0.5}F_2$:Eu^{2+}, respectively (see the spectra in figures 3(a) and 4(a)). It is evident that in this range of pressures an increase in pressure causes a relative increase of the contribution of the trapped exciton emission to the whole spectrum. According to relation (3) this observation indicates that the energy δ also increases with pressure.

This increase in δ with pressure can be expected since the negative pressure shift of the exciton emission is larger than that of the $4f^6 5d^1(e) \rightarrow 4f^7$ luminescence (see figure 5 and table 2). For the pressure ranges 36–40 kbar and 29–36 kbar for $Ba_{0.3}Sr_{0.7}F_2$:Eu^{2+} and $Ba_{0.5}Sr_{0.5}F_2$:Eu^{2+}, respectively, one observes a very rapid change of the luminescence lineshape. From relation (3) it follows that the energy δ decreases rapidly to zero and the exciton emission is replaced by $4f^6 5d^1(e) \rightarrow 4f^7$ luminescence (see figures 3(b) and 4(b)). In this pressure range the response of the system to pressure is strongly nonlinear. This is a very different behavior than in the case of BaF_2:Eu^{2+} where a decrease of δ with increasing pressure is obtained for all pressure ranges (Mahlik *et al* 2008). The nonlinear response of δ has a complex nature. It is interesting that the strong nonlinearity concerns the energy of the impurity trapped exciton. The nonlinear behavior of the energy of the Eu^{2+} trapped exciton is discussed in detail in section 5.

3.3. Time-resolved spectra and luminescence kinetics

To get information on the radiative lifetime and decay of the Eu^{2+} trapped exciton and $4f^6 5d^1(e) \rightarrow 4f^7$ luminescence we measured the kinetics of SrF_2:Eu^{2+} and $Ba_{0.3}Sr_{0.7}F_2$:Eu^{2+} emission. The ambient pressure, ambient temperature and liquid nitrogen temperature luminescence decays of SrF_2:Eu^{2+} are presented in figure 6(a). One notices that at both temperatures the decay is exponential and is equal to 0.38 μs and 0.31 μs for 80 K and room temperature, respectively.

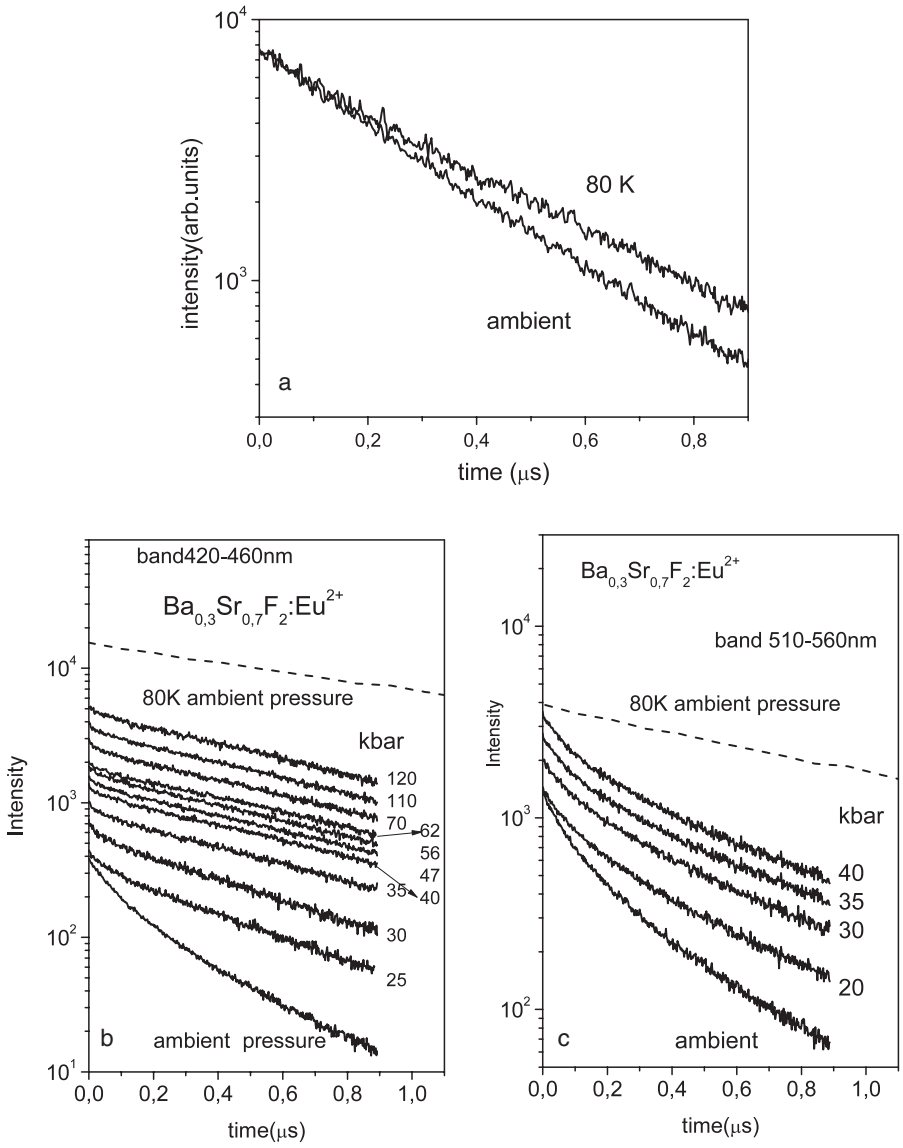

Figure 6. (a) Ambient pressure SrF_2:Eu^2 luminescence decay at 80 K and at ambient temperature. (b) Decays of the luminescence of $Ba_{0.3}Sr_{0.7}F_2$:Eu^{2+} (emission monitored 420–460 nm) at different pressures at room temperature. The dashed curve represents the luminescence at ambient pressure at 80 K. (c) Decays of the luminescence of $Ba_{0.3}Sr_{0.7}F_2$:Eu^{2+} (emission monitored 510–560 nm) at different pressures at room temperature. The dashed curve represents the luminescence at ambient pressure at 80 K. Ambient pressure results were obtained for macroscopic samples.

Since the luminescence of $Ba_{0.3}Sr_{0.7}F_2$:Eu^{2+} is a superposition of the Eu^{2+} trapped exciton and $4f^65d^1(e) \rightarrow 4f^7$ luminescence we monitored the emission in two spectral regions: the $4f^65d^1(e) \rightarrow 4f^7$ luminescence region (420–460 nm) and the exciton region (510–560 nm). The respective luminescence decays obtained at room temperature are presented in figures 6(b) and (c). For comparison the luminescence obtained at ambient pressure at 80 K is presented. The decays for a given temperature are almost the same for both spectral regions, confirming that the trapped exciton state and $4f^65d^1(e)$ state are in thermal equilibrium (see the curves representing luminescence decays obtained at ambient pressure, 20, 30 and 35 kbar in figures 6(b) and (c)).

When the decays were not a single exponential (room temperature) the average decay was defined as $\tau_R = \frac{\int I(t)t\,dt}{\int I(t)\,dt}$. For ambient pressure conditions τ_R was equal to 0.3 μs, whereas at 80 K the decay was single exponential and was equal to 1.27 μs. The decrease of the decay time with temperature is accompanied by a reduction of the luminescence (see figure 2(a)) and is related to nonradiative processes, whereas the multiexponential decay observed for room temperature is related to inhomogeneity of the sample, resulting from the inhomogeneous distribution of Eu^{2+} sites with different numbers of Ba^{2+} and Sr^{2+} ions in mixed crystals (Gatch *et al* 2006). In model presented here, this corresponds to different activation energies for nonradiative processes (energy δ_1) in different sites.

The luminescence decay times increase with pressure starting from 0.5 μs for a pressure of 25 kbar. For pressures above 40 kbar in the region 420–460 nm where the luminescence arises only from $4f^65d^1(e) \rightarrow 4f^7$, the decay time is constant and is equal approximately to 0.8 μs.

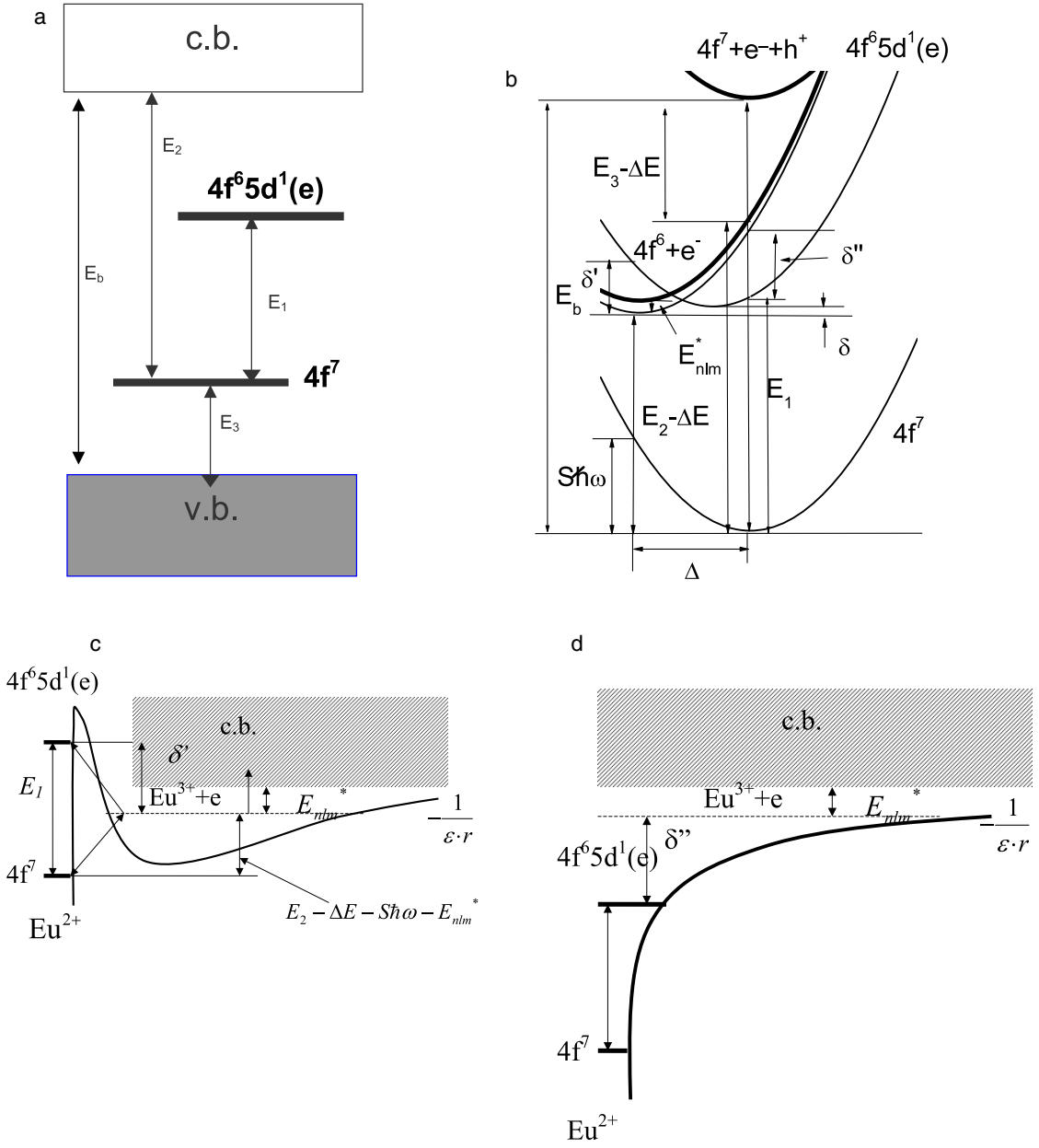

Figure 7. (a) Energy diagram of isovalent Eu^{2+} ion in fluoride crystals. (b) Configurational coordinate diagram representing the energy level structure of the Eu^{2+} ion and trapped exciton system. (c) Realistic potential for the Eu^{3+} system in the presence of a large lattice relaxation. (d) Realistic potential for the Eu^{3+} system in the absence of a large lattice relaxation (rigid lattice approximation).

It is interesting that this decay is two times longer than the decay of the $4f^65d^1(e) \rightarrow 4f^7$ luminescence in SrF_2:Eu^{2+} (0.38 μs). The $4f^65d^1(e) \rightarrow 4f^7$ transition in Eu^{2+} is parity allowed. Therefore this relatively long decay time suggests that the $4f^65d^1(e) \rightarrow 4f^7$ transition is spin-forbidden and that the transition probability is controlled by the spin–orbit interaction and is therefore sensitive to the energies of the states of different spins in the $4f^65d^1(e)$ and $4f^7$ electronic manifolds.

4. Model of Eu^{2+}-trapped exciton

In order to analyze the radiative and nonradiative processes in the system we consider the energy level structure of Eu^{2+}, presented schematically in figure 7(a). E_1 and E_2 represent the energy of internal transitions in the Eu^{2+} ($4f^65d^1(e) \leftrightarrow 4f^7$ transition) and the impurity ionization energy (creation of Eu^{3+} ion), respectively. E_3 is the energy released when a free hole from the valence band is captured by the Eu^{2+} ion and the Eu^{3+} is created.

Dorenbos (2003) has analyzed the anomalous luminescence in the context of the relation between the impurity ionization energy (represented by E_2 in figure 7(a)) and the energy of the $4f^65d^1(e)$ state (represented by E_1 in figure 7(a)). The ionization energy of the $4f^65d^1(e)$ state, $E_2 - E_1$, has been considered to be that of the free lanthanide reduced by the Madelung energy including the Pauling repulsion, the energy of lattice polarization and the electron affinity in the conduction band of the host (Dorenbos 2003).

In the present approach the system of Eu^{2+} and Eu^{2+} trapped excitons is described by the following Hamiltonian proposed by (Gryk *et al* 2005):

$$H = \frac{-\hbar^2\nabla^2}{2m} + V_{\mathrm{cr}}(\mathbf{r}) + V_{\mathrm{RE}}(\mathbf{r})|_{r<R} - \frac{e^2}{\varepsilon \cdot r} + V_{\mathrm{latt}}(\Delta, \mathbf{r}) \quad (4)$$

where V_{RE} is the local potential of the Eu^{3+} ion and V_{cr} is the lattice periodic potential. Subscripts $r > R$ and $r < R$ denote the potential outside and inside the first coordination sphere, respectively, while R is the average distance between the Eu^{2+} ion and the ligands. A hole captured at Eu^{2+} (i.e. Eu^{3+}) creates a long range Coulomb potential, $-\frac{e^2}{\varepsilon \cdot r}$.

The energy $V_{\mathrm{latt}}(\Delta, \mathbf{r})$ describes the system reaction to the ionization of Eu^{2+} into Eu^{3+} and includes the electronic energy related to delocalization of the electron and the lattice relaxation energy, and Δ is the shift of the ligands (nearest-neighbor F^- ions). In the adiabatic approximation one considers the dependence on Δ and $\mathbf{r}$ in $V_{\mathrm{latt}}(\Delta, \mathbf{r})$ as follows;

$$V_{\mathrm{latt}}(\Delta, \mathbf{r}) = V'_{\mathrm{latt}}(\Delta) + V''_{\mathrm{latt}}(\Delta, \mathbf{r}). \quad (5)$$

It has been shown (Gryk *et al* 2005) that the decrease of the electron number caused a decrease in the energy of the system and a compression of the lattice (negative Δ). One obtained

$$V'_{\mathrm{latt}}[\Delta] = -\Delta E - S\hbar\omega, \quad (6)$$

where $S\hbar\omega$ was the lattice relaxation energy:

$$S\hbar\omega = \frac{k}{2}\Delta^2 = \frac{2C^2}{kR^{2(m+1)}}, \quad (7)$$

and ΔE was the additional energy of the captured hole:

$$\Delta E = \frac{C}{R^m}. \quad (8)$$

The ligand shift is

$$\Delta = \frac{2C}{kR^{m+1}}. \quad (9)$$

The constant C and exponent m depended on the model, $m = 1$ describes the classic electrostatic potential (Madelung potential), $m = 2$ corresponds to the energy of an electron in a quantum well, $m = 5$ corresponds to the energy of an electron in a crystal field and $m = 12$ represents the inter-ionic repulsion given by the Lennard-Jones potential. Since the changes in Madelung potential are already included by consideration of dielectric screening, we assume that m should be greater than 2 and the lattice relaxation considered here concerns only the ligand ions and does not extend beyond the first coordination sphere.

The shifted ligands create the short range repulsion potential

$$V''_{\mathrm{latt}}(\Delta, \mathbf{r}) = \sum_i \frac{Z_i}{|\mathbf{r} - \mathbf{R}_i|^3}(\mathbf{r} - \mathbf{R}_i) \cdot \Delta_i. \quad (10)$$

In relation (10) the zero of the potential corresponded to the conduction band edge. To visualize relation (10) one simplifies the potential, considering it is the potential resulting from two charged spheres with radii R and $R - \Delta$, and charges $Q = \sum_i Z_i$ and $-Q$, respectively. Thus the potential

$$V''(\Delta, r) = \begin{cases} 0, & r < R - \Delta \\ \dfrac{Q}{R^2}(R - r), & R - \Delta < r < R \\ 0, & r > R. \end{cases} \quad (11)$$

The Hamiltonian (4) generates two types of states: the localized states relate to the potential V_{RE}, i.e. the $4f^7$ and $4f^6 5d^1$ states of Eu^{2+}, and the delocalized states relate to the Coulomb potential (the Rydberg states). In the effective mass approximation (Kohn 1957) the energies of the Rydberg states were related to the conduction band edge and created the hydrogen-like structure:

$$E^*_{nlm} = \frac{1}{n^2} Ry \frac{m^*}{\varepsilon^2}. \quad (12)$$

Here Ry is the Rydberg constant, m^* is the electron effective mass of the electron in the conduction band and ε is the static dielectric constant of the material. The quantum numbers n, l and m represent the hydrogen-like states. The Rydberg states are delocalized since the electron can penetrate distances larger than the lattice constant. The effective Bohr radius of the 1s state is $a^* = a_0 \frac{\varepsilon}{m^*}$.

For the purpose of further consideration, one distinguishes two types of eigen wavefunctions, $\varphi_c(\mathbf{r})$ for localized and $F_{nlm}(\mathbf{r})$ for Rydberg delocalized states. Noting that they are orthogonal:

$$\int F^*_{nlm}(\mathbf{r})\varphi_c(\mathbf{r})\,\mathrm{d}\mathbf{r} = 0. \quad (13)$$

The configurational coordinate diagram of the system described by Hamiltonian (4) is shown in figure 7(b). The lowest parabola corresponds to the $4f^7$ ground state of Eu^{2+}. The parabola labeled $4f^6 5d^1$ (e) corresponds to the excited state of the Eu^{2+} ion. The parabola labeled $4f^7 + e + h$, shifted from the ground one by energy E_b, corresponds to the excited system: the Eu^{2+} ion in the ground state and a free electron and hole in the conduction and valence bands, respectively. Parabolas labeled as $4f^6 + e$ correspond to the case in which a hole is trapped at the Eu^{2+} ion (i.e. Eu^{3+}) and the electron is in the conduction band (thick parabola), or the electron is in the Rydberg states (thin parabola). Thus the energy of the trapped exciton state is smaller than the energy of the $4f^7 + e + h$ state, $E_{b,}$ by energies $E_3 - \Delta E$, $S\hbar\omega$ and E^*_{nlm}.

To consider the realistic shift of the ligands one should discuss the meaning of C in relations (7) and (8). Its value should be considered as a product of two factors: C_0, which is related to fundamental constants, and C_1, which is related to the probability of finding a 'delocalized' electron in the core region of Eu^{3+} (a distance smaller than R). One can define

$$C_1 = 1 - \int_0^R |F_{nlm}(\mathbf{r})|^2\,\mathrm{d}\mathbf{r}. \quad (14)$$

Thus $C_1 = 1$ when the probability of finding the electron occupying the Rydberg state inside this area is equal to zero. In any other case, $C_1 < 1$, so that it reduces the energy ΔE,

the lattice relaxation energy and the ion shift Δ. The necessity for a large C_1 causes a situation such that the trapped exciton is formed with a superposition of Rydberg states with $l \geqslant 1$, whose wavefunctions are equal to zero at $r = 0$.

The realistic potential of the Eu^{3+} ion in the presence of lattice relaxation, given by the formula

$$U(\mathbf{r}, \Delta) = V_{\mathrm{RE}}(\mathbf{r})|_{r<R} - \frac{e^2}{\varepsilon \cdot r} + V''(\Delta, \mathbf{r}) \qquad (15)$$

is presented in figure 7(c). The dashed box represents continuum states (the conduction band edge corresponds to the bottom of the box). At a large distance from the Eu^{3+}, the potential, $U(\mathbf{r}, \Delta) = -\frac{e^2}{\varepsilon \cdot r}$, whereas for a short distance from the europium, the shifted ligands create a short range repulsion potential given by formula (11). The dashed line represents the level that could be occupied by the electron captured by the Coulomb potential of Eu^{3+}. For $r < R - \Delta$ we deal with the local potential of Eu^{3+} that binds the electron at the localized Eu^{2+} states. The thick solid lines represent the Eu^{2+} states: $4f^6 5d^1$(e) and ground state $4f^7$. The potential created by the shifted ligands causes an increase of the energies of Eu^{2+} by an amount equal approximately to $\frac{Q}{R^2}\Delta$ and is the energy barrier that separates the localized states of Eu^{2+} from the delocalized Rydberg states of the type $Eu^{3+} + e$. The diagram presented in figure 7(c) corresponds to an energy level structure of the system with a large lattice relaxation (for configurational coordinate equal to $-\Delta$ in the diagram presented in figure 7(b)), where the energy of the $4f^6 5d^1$(e) electronic manifold is higher than the energy of the trapped exciton by the quantity δ'. A realistic potential without lattice relaxation is shown in figure 7(d). The lack of lattice relaxation causes a situation such that the localized and delocalized states are not separated by an energy barrier. The situation of a small lattice relaxation presented in figure 7(d) corresponds to the situation in which the energy of the $4f^6 5d^1$(e) electronic manifold is smaller than the energy of the trapped exciton state by δ'' (see figure 7(b)).

To analyze the pressure dependence of the of the spectral lineshape one considers how the energies of localized and delocalized states change with pressure. The energy of the $4f^6 5d^1$(e) state diminishes with increasing pressure with respect to the ground state of the Eu^{2+} system due to an increase of the crystal field splitting of the d electronic configuration (Grinberg 2006).

To analyze the pressure dependence of the energy of the Eu^{2+} trapped exciton one calculated quantities $\frac{\mathrm{d}\Delta E}{\mathrm{d}p}$, $\frac{\mathrm{d}S\hbar\omega}{\mathrm{d}p}$ and $\frac{\mathrm{d}\Delta}{\mathrm{d}p}$. Relations (7), (8) and (9) yield

$$\frac{\mathrm{d}\Delta E}{\mathrm{d}p} = m\frac{\Delta E}{3B} \qquad (16)$$

$$\frac{\mathrm{d}S\hbar\omega}{\mathrm{d}p} = -S\hbar\omega \cdot \left[\frac{1}{k}\frac{\mathrm{d}k}{\mathrm{d}p} + 2(m+1)\frac{1}{R}\frac{\mathrm{d}R}{\mathrm{d}p}\right] = \frac{S\hbar\omega}{3B}[2(m+1) - 6\gamma] \qquad (17)$$

and

$$\frac{\mathrm{d}\Delta}{\mathrm{d}p} = -\Delta \cdot \left[\frac{1}{k}\frac{\mathrm{d}k}{\mathrm{d}p} + (m+1)\frac{1}{R}\frac{\mathrm{d}R}{\mathrm{d}p}\right] = \frac{\Delta}{3B}[(m+1) - 6\gamma] \qquad (18)$$

where B is the local bulk modulus of the material and γ is the Grüneisen parameter.

An increase in pressure causes an increase of the absolute value of the energy ΔE (relations (8) and (16)) since it diminishes the central ion–ligand distance. It diminishes the energy of the Eu^{2+} trapped exciton with an increase in pressure. The influence of pressure on the lattice relaxation energy is ambiguous. Relation (17) represents the superposition of two effects; the increase of $S\hbar\omega$ due to the decrease of R (the positive contribution) and the decrease of $S\hbar\omega$ due to an increase in the elastic constant (the negative contribution). As a result the electron–lattice interaction energy has been usually considered as weakly dependent on pressure (Grinberg 2006). Since the energy of the $4f^6 5d^1$(e) electronic manifold also decreases with pressure, both situations are possible: an increase in pressure can cause either the $4f^6 5d^1$(e) electronic manifold-exciton level to undergo a crossing or the crossing will not occur.

5. Nonlinear changes of energy of Eu^{2+} trapped exciton with pressure

In the case of mixed $Ba_xSr_{1-x}F_2$:Eu^{2+} ($x = 0.3$ and 0.5) crystals, pressure causes a reduction in the energy of the anomalous luminescence as well as that of the $4f^6 5d^1$(e) $\rightarrow$ $4f^7$ transition in Eu^{2+}, but the energy difference between the $4f^6 5d^1$(e) and exciton states increases with pressure. However, in all cases, at pressures above 50 kbar, the anomalous luminescence is replaced by the normal one. Whereas the $4f^6 5d^1$(e) $\rightarrow$ $4f^7$ transition energy decreases linearly with increasing pressure, the anomalous luminescence transition energy change is strongly nonlinear above a critical pressure. Such nonlinear behavior can be attributed to the phase transition observed in fluorides at pressures between 30 and 50 kbar, but still one cannot unambiguously relate the type of luminescence to the specific phase. For BaF_2:Eu^{2+} and mixed $Ba_xSr_{1-x}F_2$:Eu^{2+} crystals both the anomalous and normal luminescence occurs simultaneously in the cubic and orthorhombic phases, respectively. On the other hand, in SrF_2:Eu^{2+} only normal luminescence occurs, regardless of phase.

One can summarize the known experimental results as follows:

(1) In materials where at ambient pressure one observes the $4f^6 5d^1$(e) $\rightarrow$ $4f^7$ transition (SrF_2:Eu^{2+} (Gatch *et al* 2006) and CaF_2:Eu^{2+} (Troster *et al* 2002)) only this luminescence is observed for all pressures independent of phase (cubic or orthorhombic).
(2) The energy of the $4f^6 5d^1$(e) $\rightarrow$ $4f^7$ transition decreases linearly with pressure and the phase transition does not influence this dependence in the case of BaF_2:Eu^{2+} and mixed $Ba_xSr_{1-x}F_2$:Eu^{2+} crystals. This is in full accordance with the prediction of the crystal field model (Grinberg 2006).
(3) The energy of the anomalous luminescence peak (recombination of trapped exciton) decreases with pressure for small pressures. This is in accordance with

Table 3. Properties of BaF_2 and SrF_2. The experimental data, when available are listed in the first row.

	BaF_2		SrF_2	
	Cubic	Orthorhombic	Cubic	Orthorhombic
Bulk modulus (kbar)	570 (Leger *et al* 1995) 796.4 (Kanchana *et al* 2003a)	790 ± 100 913.9 (Kanchana *et al* 2003a)	690 (Samara 1976) 903.5 (Kanchana *et al* 2003b)	— 1270 (Kanchana *et al* 2003b)
Bandgap (eV)	9.1 (Harrison 1980) 7.03 (Kanchana *et al* 2003a)	— 7.16 (Kanchana *et al* 2003a)	— 7.55 (Kanchana *et al* 2003b)	— 8.24 (Kanchana *et al* 2003b)
Dielectric constant	7.34 (Samara 1976)		6.48 (Samara 1976)	
Pressure of phase transition (kbar)	30 (Leger *et al* 1995)		50 (Francisco *et al* 2002)	

the proposed model of the Eu^{2+} trapped exciton (the changes in the energy ΔE given by relation (16) are larger than the changes of $S\hbar\omega$ given by relation (17)).

(4) In the case of $Ba_xSr_{1-x}F_2$:Eu^{2+} ($x = 0.5$ and 0.3) the transition from anomalous to normal luminescence is very rapid and takes place due to the nonlinear dependence (rapid increase) in the energy of the trapped exciton state on pressure. This is not the case for BaF_2:Eu^{2+}.

(5) In $Ba_xSr_{1-x}F_2$:Eu^{2+} ($x = 0$, 0.3 and 0.5) in the orthorhombic phase only the normal $4f^65d^1(e) \rightarrow 4f^7$ emission is observed.

One can use the model of the impurity trapped exciton to explain the nonlinear dependence of the energy of the trapped exciton on pressure. Let us consider the case when the energy of the trapped exciton is lower than the energy of the $4f^65d^1(e)$ state at ambient pressure. Under ambient conditions the system is characterized by a large lattice relaxation and the wavefunction of the electron at the trapped exciton Rydberg states, F_{nlm}, does not penetrate the core region of the Eu^{3+} ion.

One considers the effect of pressure as a perturbation. The energy of the trapped exciton state decreases with increasing pressure due to an increase in the energy ΔE. One can make the realistic assumption that the electron–lattice interaction does not depend on pressure. Thus from relations (17) and (18) when $[2(m+1) - 6\gamma] = 0$ the quantity $[(m+1) - 6\gamma] < 0$. As a result, one expects that the pressure reduces the shift of the ligand ions, Δ. A decrease of Δ causes a decrease of the energy barrier given by relation (11). According to the perturbation approach, reducing the energy barrier causes the mixing of Rydberg and localized states. Specifically the modified Rydberg states contains some admixture of the localized wavefunctions:

$$F'_{nlm} = b_0 F_{nlm} + \sum_c b_c \varphi_c. \tag{19}$$

For the function given by (19) the relation (14) causes a decrease of C_1 and an additional decrease of the ligand energy shift, ΔE, the electron lattice relaxation energy $S\hbar\omega$, and the potentials $V'_{\text{latt}}(\Delta)$ and $V''_{\text{latt}}(\Delta, r)$. The mixing of the Rydberg and $4f^7$, and $4f^65d^1(e)$ states is stronger for these d-like states occurring in the excited states than for the more localized f-states found in the ground state.

The effect described above becomes nonlinear with pressure and yields the steep increase in the energy of the Eu^{2+} trapped exciton with respect to the $4f^65d^1(e)$ and $4f^7$ states. The realistic potential for no shift of the ligands (or small ion shift) looks like the one presented in figure 7(d). In this case the Rydberg states still exist; however, they do not contribute to the luminescence due to fast nonradiative relaxation to the $4f^65d^1(e)$ state.

6. Conclusions

The pressure and temperature dependence of the luminescence of Eu^{2+}-doped fluoride crystals $Ba_xSr_{1-x}F_2$ ($x = 0$, 0.3, 0.5 and 1) were analyzed. A strongly nonlinear dependence of the energy of the Eu^{2+} trapped exciton on pressure in the case of $Ba_{0.3}Sr_{0.7}F_2$:Eu^{2+} and $Ba_{0.5}Sr_{0.5}F_2$:Eu^{2+} was observed. This effect could not be explained by a simple model in which pressure causes changes in the energy levels resulting only from changes in the volume of the crystal.

A model of the Eu^{2+} trapped exciton was developed. In this model a crucial role is played by the local lattice relaxation (the compression of the Eu-ligand system) considered as the lattice response to Eu^{2+} ionization. It was shown that ligand shifts created the short range repulsive potential that separated the core states of Eu^{2+} from delocalized Rydberg states of the $Eu^{3+} + e$ system and stabilized the Eu^{2+} trapped exciton system.

The influence of pressure on the trapped exciton state can be different at different pressures. According to our experimental data, for small pressures, increasing the pressure caused a reduction of the energy of the trapped exciton due to an increase in the energy (ΔE). In the high pressure regime, an increase of bulk modulus and elastic constant caused a decrease of the energy barrier $V''(\Delta, r)$ and a rapid increase in the energy of the trapped exciton accompanied by a decrease of the lattice relaxation energy. The latter effect was strongly nonlinear. In such a way an increase of pressure destabilized the Eu^{2+} exciton state due to quantum mixing of the excited states of Eu^{2+}—the $4f^65d^1(e)$ and Rydberg states of $Eu^{3+} + e$ system.

The quantities that contributed to the formation of the trapped exciton states were the bandgap energy, electron effective mass, dielectric constant and bulk modulus. The electron effective masses in these fluorides have not been estimated. The other available quantities for BaF_2 and SrF_2 are presented in table 3. One notices that the bulk modulus

increases when the system is transformed from the cubic to orthorhombic phase. The bandgap has the same behavior. The bandgap and bulk modulus are larger in the case of SrF_2 than in BaF_2. The dielectric constant of SrF_2 is smaller than that of BaF_2. Therefore conditions in the orthorhombic phase are not favorable for the creation of impurity trapped excitons and anomalous luminescence

The pressure-induced phase transformation (cubic to orthorhombic) yields a reduced crystal volume resulting in a decrease in the ligand shift, Δ; this causes the destruction of the Eu^{2+} trapped exciton states.

In the paper (Gatch *et al* 2006) the differences in the luminescence lineshapes between BaF_2:Eu^{2+}, SrF_2:Eu^{2+} and $Ba_xSr_{1-x}F_2$:Eu^2 were discussed considering the inhomogeneous distribution of Eu^{2+} sites with different numbers of Ba^{2+} and Sr^{2+} ions in mixed crystals. The discussion and conclusions presented in this paper (Gatch *et al* 2006) are still valid. In the case of $Ba_{0.3}Sr_{0.7}F_2$:Eu^{2+} and $Ba_{0.5}Sr_{0.5}F_2$:Eu^{2+} we deal with various Eu^{2+} sites that differ in the number of Ba^{2+} ions in the second coordination sphere. As a result, the luminescence of different sites is transformed from anomalous to normal at slightly different pressures.

Acknowledgment

This paper has been supported by grants of the Polish Ministry of Science and Higher Education in years 2008–2011.

References

Dorenbos P 2003 *J. Phys.: Condens. Matter* **15** 2645
Dujardin C, Moine B and Pedrini C 1992 *J. Lumin.* **53** 444
Dunstan D J and Spain I L 1989 *J. Phys. E: Sci. Instrum.* **22** 913
Francisco E, Blanco M A and Palacios P 2002 *Int. J. High Pressure Res.* **22** 227
Gatch D B, Boye D M, Shen Y R, Yen Y M, Grinberg M and Meltzer R S 2006 *Phys. Rev.* B **74** 195117
Grinberg M 2006 *Opt. Mater.* **28** 26
Gryk W, Dyl D, Ryba-Romanowski W and Grinberg M 2005 *J. Phys.: Condens. Matter* **17** 5381
Harrison W A 1980 *Electronic Structure and Properties of Solids* (San Francisco, CA: Freeman)
Hernández I and Rodriguez F 2003 *Phys. Rev.* B **67** 012101
Kanchana V, Vaitheeswaran G and Rajagopalan M 2003a *J. Alloy Compounds* **359** 66
Kanchana V, Vaitheeswaran G and Rajagopalan M 2003b *Physica* B **328** 283
Kim J S, Park Y H, Kim S M, Choi J C and Park H L 2005 *Solid State Commun.* **133** 445
Kohn W 1957 *Solid State Phys.* **5** 257
Kourouklis G A and Anatassakis E 1986 *Phys. Rev.* B **34** 1233
Leger J M, Haines J, Atouf A, Schuete O and Hull S 1995 *Phys. Rev.* B **52** 13247
Mahlik S, Kukliński B, Yen Y M, Meltzer R S and Grinberg M 2008 *J. Lumin.* **128** 715
McClure D S and Pedrini C 1985 *Phys. Rev.* B **32** 8465
Merrill L and Bassett W A 1974 *Rev. Sci. Instrum.* **45** 290
Moine B, Dujardin C and Pedrini C 1994 *J. Lumin.* **58** 339
Moine B, Pedrini C and Courtois B 1991 *J. Lumin.* **50** 31
Pedrini C, McClure D S and Anderson C H 1979 *J. Chem. Phys.* **70** 4959
Pedrini C, Pagost P O, Madej C and McClure D S 1981 *J. Physique* **42** 323
Poot S H and Blasse G 1997 *J. Lumin.* **72** 247
Reut E G 1978 *Opt. Spectrosk.* **40** 55
Rodriguez F, Hernández I, Moreno M and Alcala R 2003 *J. Chem. Phys.* **119** 8686
Samara G A 1976 *Phys. Rev.* B **13** 4529
Shannon R D 1976 *Acta Crystallogr.* A **32** 751
Smet P F, van Haecke J E, Loncke F, Callens F and Poelman D 2006 *Phys. Rev.* B **74** 035207
Troster T H, Schweizer S, Secu M and Spaeth J-M 2002 *J. Lumin.* **99** 343